Original Article

Protective effects of baffles with different positions, row spacings, heights on debris flow impact

SUN Xinpo[1,6†] https://orcid.org/0009-0003-8363-1413; e-mail: xinpohd@suse.edu.cn

CHEN Min[1,6] https://orcid.org/0009-0006-1522-2951; e-mail: 322085607110@stu.suse.edu.cn

BI Yuzhang[2,6†] https://orcid.org/0000-0003-2631-6620; e-mail: byz690@yeah.net

ZHENG Lu[3] https://orcid.org/0000-0003-3674-2148; e-mail: zheng8211@163.com

CHE Chi[4,6] https://orcid.org/0009-0000-1143-5083; e-mail: chechi@seu.edu.cn

XU Ao[1,6] https://orcid.org/0009-0000-3957-2522; e-mail: 32108560707@stu.suse.edu.cn

TIAN Zijian[5] https://orcid.org/0009-0009-4539-0819; e-mail: imzijian7@163.com

JIANG Zheyuan[4,6*] https://orcid.org/0000-0002-8207-3478; e-mail: jiangzheyuan@seu.edu.cn

*Corresponding author

†These authors contributed equally to this work

1 College of Civil Engineering, Sichuan University of Science and Engineering, Zigong 643000, China

2 College of Resources and Environment, Fujian Agriculture and Forestry University, Fuzhou 350002, China

3 School of Civil Engineering, Fuzhou University, Fuzhou 350108, China

4 Jiangsu Key Laboratory of Urban Underground Engineering & Environmental Safety, Institute of Geotechnical Engineering, Southeast University, Nanjing 210096, China

5 Beijing Urban Construction Science Technology Promoting Association, Beijing 100055, China

6 SUSE-BZ Geoenvironmental Engineering Joint Laboratory, Sichuan University of Science and Engineering, Zigong 643000, China

Abstract: The baffle effectively slowed down debris flow velocity, reduced its kinetic energy, and significantly shortened the distance of debris flow movement. Consequently, they are widely used for protection against natural hazards such as landslides and mudslides. This study, based on the three-dimensional DEM (Discrete Element Method), investigated the impact of different baffle positions on debris flow protection. Debris flow velocity and kinetic energy variations were studied through single-factor experiments. Suitable baffle positions were preliminarily selected by analyzing the influence of the first-row baffle position on the impact force and accumulation mass of debris flow. Subsequently, based on the selected baffle positions and four factors influencing the effectiveness of baffle protection (baffle position (P), baffle height (h), row spacing (S_r), and angle of transit area (α)), an orthogonal design was employed to further explore the optimal arrangement

of baffles. The research results indicate that the use of a baffle structure could effectively slow down the motion velocity of debris flows and dissipate their energy. When the baffle is placed in the transit area, the impact force on the first-row baffle is greater than that when the baffle is placed in the deposition area. Similarly, when the baffle is placed in the transit area, the obstruction effect on debris flow mass is also greater than that when the baffle is placed in the deposition area. Through orthogonal experimental range analysis, when the impact on the first row of baffles is used as the evaluation criterion, the importance of each influencing factor is ranked as $\alpha > P > S_r > h$. When the mass of debris flow behind the baffle is regarded as the evaluation criterion, the rank is changed to $P > \alpha > S_r > h$. The experimental simulation results show that the optimal baffle arrangement is: P_5, $S_r=16$, $\alpha=35°$, $h=9$.

Keywords: Debris flow; Baffle; Protective effect; Discrete element

1 Introduction

Debris flow is a multiphase fluid phenomenon caused by rock collapses and falling rocks. Its high-speed movement carries significant kinetic energy, making it highly destructive. According to the research by Scheidl et al. (2023), the volume range of debris flow is typically between 0.4×10^6 - 1×10^9 m³. Debris flows often cause severe damage to transportation infrastructure such as roads and railways, as well as to villages and towns, resulting in casualties and economic losses (Zhu et al. 2020). To protect downstream environments, ecosystems, and society, researchers commonly employ engineering structures along predicted debris transit areas, including check dams, slit dams, flexible baffles, and baffles. Baffle arrangements are flexible, construction equipment is simple, the construction process is convenient, safe, and the project duration is short with a small scale (Zhou et al. 2019; Song et al. 2018). Baffles installed along the transit area of debris flows are crucial forms of protection against debris flow disasters (Bi et al. 2016). The primary function of the baffles was to reduce the flow velocity of the debris flow and dissipate its kinetic energy, thereby enhancing its protective effect. When the debris flow passed through the interlaced baffles, it was impeded by the baffle structure (Cheng et al. 2022). Additionally, mutual interference among debris flows can also reduce their velocity. Due to the obstructive role of the baffles structure, a significant amount of kinetic energy of debris flows is dissipated, and some debris flows are prevented from moving further downstream. Therefore, baffles are considered effective protective structures for reducing the volume and mobility of debris flows.

A proper baffle design can effectively improve the protective effect of the baffles. To explore the effects of different baffle arrangements on debris flows, and considering the high cost, design complexity, and long duration of real-scale debris flow model experiments, many scholars chose to conduct small-scale flume model experiments. Specific flume model experiments are listed in Table 1. Bi et al. (2021) investigated the interception effects of arc-shaped baffles and conventional baffles (cylindrical and square baffles) from three aspects: debris flow deposition area, velocity reduction rate, and dimensionless velocity through flume model experiments. Kim and Yune (2020) studied the effects of baffles with different heights and row numbers on debris flow velocity and kinetic energy based on flume model experiments. Wang et al. (2017) analyzed the effects of debris flow density, baffle shape, and spacing on debris flow velocity and energy loss through flume model experiments, revealing that the velocity reduction rate increased with density, while it was inversely proportional to the equivalent impact area and spacing between adjacent rows. Yang et al. (2021) investigated the effects of particle size, flow area angle, baffle spacing, and row numbers on energy dissipation, travel distance, and impact forces on baffles through flume model experiments, finding that smaller debris flows favored frictional energy dissipation, resulting in shorter travel distances.

Numerical simulation, as one of the important methods for studying geological disasters, has been widely used to explore the movement mechanisms of debris flows and barriers (Zhu et al. 2018; Liu et al. 2019; Zhang et al. 2019). The numerical simulation based on the scale of the flume model has several advantages. Firstly, the results from flume models can be verified against numerical simulation results, ensuring the accuracy and reliability of the research findings. Secondly, it allows for in-depth analysis of interactions, revealing underlying mechanisms and patterns. Additionally, continuously enriching the case results contributes to obtaining more comprehensive

Table 1 Summary of previous studies on the baffles under debris flow

| References | Types | Baffles | | | Angle of transit area (°) | Baffle shape | Objective |
		Position	Height (cm)	Row spacing (cm)			
Wang et al. (2020)	FM	Deposition area	18	5, 7, 9, 11	35°	Cylindrical baffle, square baffle, arc-shaped baffle	Velocity, accumulation pattern
Bi et al. (2021)	FM	Deposition area	18	5, 7, 9,11	35°	Square baffle, arc-shaped baffle, cylindrical baffle	Velocity, kinetic energy, accumulation pattern
Bi et al. (2023)	FM	Transit area	18	9	35°	Cylindrical baffle, square baffle	Velocity, accumulation form and mass, blocking rate
Bi et al. (2022)	FM	Deposition area	18	3, 5, 7, 9, 11	35°	Cylindrical baffle	Velocity, kinetic energy
Choi et al. (2014)	FM	Transit area	6, 8,12	5, 10	26°	Square baffle	Flow velocity, kinetic energy
Kim et al. (2019)	FM	Transit area	2, 4, 6, 8	20	29°	Cylindrical baffle	Flow velocity, flow depth
Kim and Yune (2020)	FM	Transit area	4, 6, 8	20	29°	Cylindrical baffle, square baffle	Flow depth, velocity, kinetic energy
Wang et al. (2017)	FM	Transit area	-	10, 15, 25	12°	Square baffle, trapezoidal baffle, triangular prism baffle	Flow velocity, kinetic energy
Zhang et al. (2021)	NS	Transit area, deposition area	10	6	45°	Square baffle	Kinetic energy, impact force, number of debris flow, accumulation form and movement distance
Huang et al. (2021)	NS	Transit area	35	21	40°	Square baffle, triangular prism baffle	Kinetic energy, impact force, accumulation form and mass
Zhang and Huang (2022)	NS	Deposition area	17	-	30°	Square baffle	Velocity, impact force, accumulation pattern
Chen et al. (2022)	NS	Transit area	10, 20	9	30°, 35°, 40°, 45°	Square baffle	Velocity, impact force
Bi et al. (2018)	NS	Transit area	50, 60	6, 18, 30	20°, 50°	Square baffle	Velocity, impact force
Zhou et al. (2019)	NS	Transit area	200	-	20°	Square baffle	Velocity, debris flow movement height
Luo et al. (2023)	NS, FM	Transit area	10, 20 30	-	30°	Square baffle, arc-shaped baffle, triangular prism baffle	Velocity, debris flow mass, trajectory and accumulation pattern

Notes: FM=Flume model; NS=Numerical simulation.

data support and verifying conclusions. Finally, through continuous optimization of experimental design and methods in numerical simulations, the research cost can be further reduced, and research efficiency and sustainability can be improved. Therefore, many scholars choose to adopt numerical simulation methods based on flume models. This approach can simulate the dynamic transition process of debris flows from stable to unstable states and potentially predict the areas affected by debris flows. Numerical models mainly include two types: the continuous and discontinuous medium models. Continuum models assume that fragment materials are continuous, and their dynamics are entirely controlled by continuum theory. This model has advantages such as technical maturity, theoretical

soundness, high computational efficiency, and wide applicability. Therefore, it has been widely used to analyze landslide characteristics (Moretti et al. 2020; Cuomo et al. 2021). For example, Cuomo et al. (2017) used Smoothed Particle Hydrodynamics (SPH) to calculate time reasonably and accurately describe the main kinematic quantities. Cuomo and Petrosino (2020) simulated the propagation scenarios of different induced fragment avalanches under the action of two engineering slopes using the Smoothed Particle Hydrodynamics (SPH) method. Although continuum models can reflect the characteristics of debris flow movement and deposition, they cannot describe the interaction mechanisms between solid particles in detail. In contrast, discrete element models can not only capture the overall dynamic

characteristics of granular materials but also explore the gradual failure of particles during motion. Among them, the Discrete Element Method (DEM) is one of the most widely used discrete element models (Zhao et al. 2017; Liu et al. 2018; Lei et al. 2020). Zhao et al. (2015) used the CFD-DEM coupling method to study the influence of particle impact on water wave generation, and their results were consistent with field observation results. Gan et al. (2018) simulated failure characteristics using PFC 2D, and their numerical results matched well with experimental data. These studies indicate that the discrete element method can accurately and effectively simulate the dynamic characteristics of loose granular flow in narrow channels. Specific numerical simulation experiments are shown in Table 1. Bi et al. (2018) detailed the use of the DEM for numerical simulations to investigate the impact forces of debris flow on baffles with varying numbers and spacing of rows and columns. Zhou et al. (2019) employed the DEM to study the influence of Froude number and baffles row spacing on the impact of debris flow on baffles height. Zhang et al. (2021) utilized the DEM to study the arch-shaped structure between baffles at the particle scale and further analyzed the impact of the Froude number on the interaction between debris flow and baffles.

According to the data in Table 2, Choi et al. (2014) and Wang et al. (2017) positioned baffles in the transit area and, based on changes in debris flow velocity and kinetic energy, investigated the effects of baffle height, row spacing, and baffle shape on debris interception. Baffles were positioned in the deposition area by Bi et al. (2022), with column spacing, row spacing, and the

number of baffles as indicators, determining the optimal baffle layout. The study indicated that baffles could be positioned either in the transit area or in the deposition area, but there is limited in-depth research on the specific placement of baffles. Kim et al. (2019), based on flume model experiments, explored the dissipation effect of baffle height and row number on debris flow energy. The results showed that baffles significantly reduced debris flow velocity and depth, and the energy dissipation effect increased with the increase in baffle height and row number. According to the data in Table 2, the range of baffle heights was between 2-30 cm, with 18 cm being a common setting. Wang et al. (2020a), using different types of baffles, determined the optimal baffle shape, studying the effects of baffle row spacing and baffle spacing on debris flow interception. The optimization of baffle placement was done through debris flow deceleration ratio and deposition area. The research range associated with baffle row spacing was between 3-25 cm, based on the data in Table 2. Cheng et al. (2022) utilized numerical simulation methods to investigate the impact of baffle height and flow direction angle on the interaction between granular flow and baffles. The results showed that reducing the transit area angle and increasing baffle height effectively lowered debris flow velocity and impact force. According to the data in Table 2, the research range for flow direction angle was 12°-45°, with 35° being a common setting. It is important to note that past studies primarily relied on flume model experiments or numerical simulation methods, analyzing the impact of single-factor variables (such as baffle shape, flow direction angle, and layout between baffles) on the interaction between debris flow and baffles, including velocity, energy, impact force, as well as the influence on debris flow form and mass. Past research lacked studies on the optimal baffle configurations for debris flow protection based on multi-factor designs, including variables such as baffle position, baffle height, baffle row spacing, and transit area angle.

To enhance the protective effect of the baffles, a three-dimensional model of debris flow impacting the baffles was constructed using the DEM in this study. The debris flow process and accumulation were simulated through single-factor experiments, investigating the impact of baffles at different positions on the changes in debris flow velocity and kinetic energy. By analyzing the impact force on the first row of baffles and the mass and form of the accumulated

Table 2 Parameters adopted in numerical simulations

Material parameters	Value
Particle diameter, θ (mm)	10
Particle density, ρ_1 (kg·m^{-3})	2100
Shear model of particle, G_S (GPa)	0.8
Baffle/flume density, ρ_2 (kg·m^{-3})	7900
Shear mlus of baffle/flume, G_o (GPa)	70
Baffle position, P	$P_1, P_2, P_3, P_4, P_5, P_6$
Angle of transit area, α (°)	30, 35, 40, 45
Baffle height, h (cm)	9, 18, 27
Baffle row spacing, S_r (cm)	8, 16, 24
Contact parameters	Value
Coefficient of restitution	0.6
Particle friction coefficient, u_1	1.33
Particle rolling friction coefficient, u_{r1}	0.15
Baffle/flume friction coefficient, u_o	0.453
Baffle/flume rolling friction coefficient, u_{ro}	0.05
Gravitational acceleration, g (m/s²)	9.81

debris flow, the interaction process between debris flow and baffles at different positions was explained, and the baffle positions were preliminarily screened. Based on this, an orthogonal experiment was conducted to study the joint effects of baffle height, row spacing, and transit area angle on the effectiveness of debris flow interception. Factors influencing the baffle interception effectiveness, such as debris flow velocity, kinetic energy, impact force on the first row of baffles, as well as the form and mass of accumulation, were analyzed. Mean and range analyses of the impact force on the first row of baffles and the mass of debris flow behind the baffles were performed to determine the degree of influence of each factor on the results and the optimal baffle arrangement. The research results contribute to a deeper understanding of the interaction between debris flow and baffles, enhancing the reliability of baffle system design.

2 Methodologies

2.1 Discrete element method

The Discrete Element Method (DEM) was a dynamic numerical analysis method capable of simulating the heterogeneity, discontinuity, and large deformations of slope rock masses. It was a popular numerical method for analyzing the stability of soil and rock masses and had been widely applied in the study of interactions between debris flows and baffles. Discrete Element Method Simulation Software (EDEM) is a simulation analysis software based on the discrete element method (DEM) and is widely used in the production process of particle processing and manufacturing equipment. Users can customize parametric models as needed and input forces, material properties, and other physical properties to establish a personalized model processing environment. With its particle factory technology and powerful computing power, EDEM is able to effectively simulate the movement process of landslide debris flow (Zhang et al. 2022; Pu et al. 2023; Huang et al. 2023). The contact model used in this study is the Hertz-Mindlin model. The choice of this contact model is because particle interactions are inherently nonlinear (Cheng et al. 2020).

The model in this paper is built upon prior indoor experiments (Wang et al. 2020b) (Fig. 1), and establishes a numerical model experiment based on

Fig. 1 Flume model used in this study.

the dimensions of a flume model, primarily encompassing the source area, transit area, deposition area, and baffle protection structure. The source area was composed of a rectangular storage box measuring 0.4 m in length, 0.3 m in width, and 0.4 m in height, with a capacity of 0.048 m³, where the debris flow mass of 60 kg was set. An inclined arc-shaped plate was installed at the bottom of the box to increase the initiation angle of the particles, ensuring that all particles could quickly flow out of the box and avoid residual particle accumulation in the source area. The flow area was a channel with a length of 4 m, a width of 0.3 m, and side walls 0.4 m high, simulating the flow characteristics of flume-type debris flow. The buffering deposition area was a square platform with a side length of 2 m, and protective structures were arranged along the platform's edges. The overall experimental setup, combining the terrain and total amount of particles, was within the range of the accumulation plane, meeting the requirements of the experiment. Square baffles with a side length of 5 cm were used as baffles. Based on existing flume experiments, a three-dimensional numerical model was constructed using the commercial software EDEM, and six sets of baffles were arranged according to the layout shown in Fig. 2. The main EDEM input parameters for this experiment are listed in Table 2 (Goodwin et al. 2021). Using EDEM's powerful post-processing capabilities, average particle velocities (v) and kinetic energies (k) throughout the particle motion process were exported, and the total impact force (f) exerted by all particles on the first row of baffles was measured.

2.2 Experimental method

A model of debris flow impacting baffles was constructed using the Discrete Element Method (DEM)

in this study. According to the data in Table 1, the baffle height is typically set between 6 and 60 cm, the inter-row spacing ranges from 6 to 30 cm, and the angle of the transit area varies from 12° to 50°.

First, single-factor experiments were conducted, setting up six groups of identical baffles P_{1-6} and a group of baffle-free particle simulation P_0 at different positions along the debris flow path for numerical simulation. The baffle height was fixed at 18 cm with a spacing of 9cm between rows, and the angle in the flow area was set at 30°. The locations of the baffles are shown in Fig. 2, where four sets of baffles were placed in the flow area at positions P_1, P_2, P_3, and P_4, located at distances of 0.6 m, 1.2 m, 2 m, and 2.8 m from the source area, respectively. In the deposition area, two sets of baffles were placed at positions P_5 and P_6, positioned 0.2 m and 0.4 m above the bottom of the transit area, respectively. Through the single-factor experiment, three sets of representative baffle positions were preliminarily selected.

Orthogonal experimental design was employed to study and process multi-factor experiments. This is a scientific method that selects a few representative experiments from numerous experimental schemes. By analyzing the results of these experimental schemes, optimal solutions can be inferred, and more information about each factor can be obtained. Orthogonal design allows the selection of the optimal baffle layout with the least number of experimental runs. Secondly, through orthogonal design, four parameters were studied: baffle position P, angle of transit area α (35°, 40°, 45°), row spacing S_r (8 cm, 16 cm, 24 cm), and baffle height h (9 cm, 18 cm, 27 cm), forming an L9(3⁴) orthogonal experimental table. Three groups of transit area angles, 35°, 40°, and 45°, are set up with no baffles for comparison. *Cases* 1-9 are baffle group design experiments under the influence of multiple factors, while *Controls* 1-3 are baffle-free
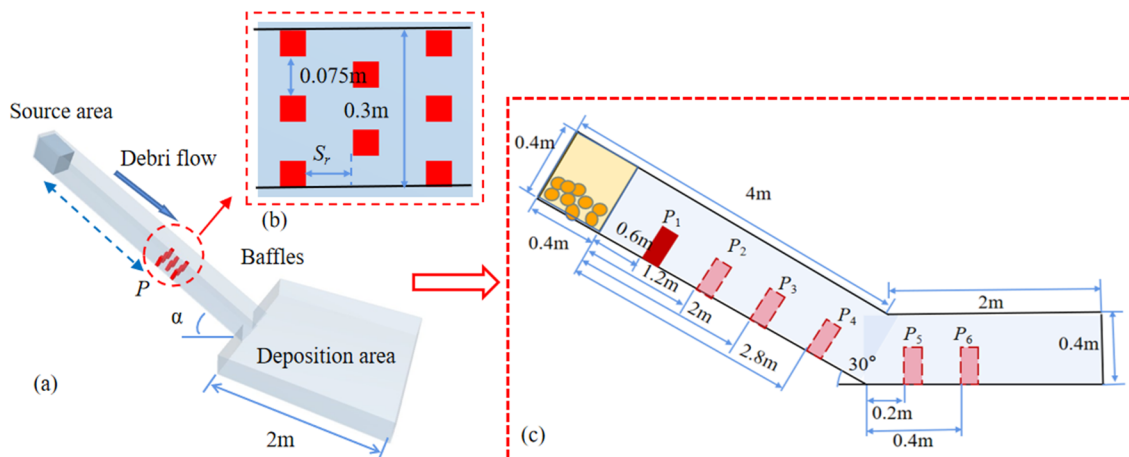
Fig. 2 (a) Flume model in EDEM software; (b)Baffles layout position in EDEM software via vertical view; (c) Flume model in EDEM software via front view.

Table 3 Orthogonal experimental design and results

Case	Baffle position	S_r (cm)	h (cm)	α (°)	f (N)	m (kg)	Mass of debris flow (kg) in the transit area	in the deposition area
Case 1	P_3	8	9	35	78.80	7.3200	7.28	52.72
Case 2	P_3	16	18	40	126.70	17.5500	16.06	43.94
Case 3	P_3	24	27	45	218.72	26.7600	16.20	43.80
Case 4	P_4	8	18	45	152.20	24.7620	15.48	44.52
Case 5	P_4	16	27	35	68.35	5.8560	2.95	57.05
Case 6	P_4	24	9	40	117.37	15.4020	9.66	50.34
Case 7	P_5	8	27	40	67.33	1.5435	42.71	17.29
Case 8	P_5	16	9	45	86.44	1.6761	51.33	8.67
Case 9	P_5	24	18	35	46.77	0.7125	25.18	34.19
Control 1	0	0	0	35	0	0	49.00	11.00
Control 2	0	0	0	40	0	0	53.67	6.33
Control 3	0	0	0	45	0	0	54.07	5.93

Note: S_r, Baffle row spacing; h Baffle height; α, Angle of transit area; f, Maximum impact force of the 1st row baffle; m, Mass of debris flow behind the baffles.

particle simulation experiments as shown in Table 3. The influence of these four factors on the protective effect of baffles against debris flow was studied. To explore the impact of these four factors on the protective effect of baffles in depth, nine experimental groups were designed. Factors affecting the blocking effect of the baffles were analyzed, including the velocity of the debris flow, kinetic energy, the impact force of the first row of baffles, as well as the accumulation form and mass of the debris flow. Through mean and range analysis of the impact force on the first row of baffles and the debris flow mass behind the baffles, the influence of each factor on the results was determined, and the optimal baffle layout was identified. By optimizing the parameters of the baffle layout, the aim is to achieve the best protective effect. The flowchart is shown in Fig. 3.
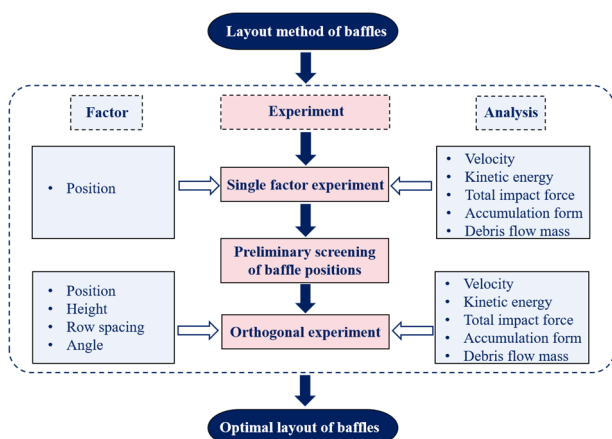
Fig. 3 Research flow chart of the optimal layout of baffles.

3　Results and Analysis

3.1 Single factor experimental study based on baffle position

3.1.1 Debris velocity and flow energy loss caused by baffles

Fig. 4(a) shows that the velocity of the debris flow changes in multiple stages under the influence of baffles at different positions. Debris flow was subjected to gravitational acceleration, and then, as it approached the barrier positions, some fluid began to decelerate, eventually reducing its speed to zero. Yang et al. (2014) mentioned that the average velocity of the real debris flow was 6 m/s to 34 m/s, however, the maximum velocity shown in Fig. 4(a) was 2 m/s. Due to the numerical simulation in this paper being based
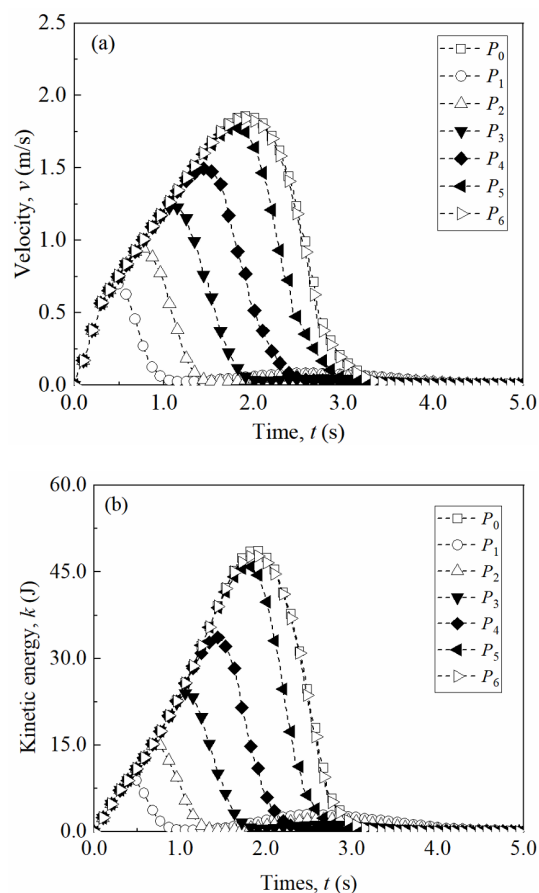
Fig. 4 (a) Velocity and (b) kinetic energy of debris flow with different baffle positions.

on a small-scale flume model, there was a scale effect, resulting in a lower simulated velocity of the debris flow compared to the actual situation. Curve P_0 represents the velocity curve without baffles, showing that particles were in an accelerating state until 2 seconds, reaching a maximum speed of 1.7 m/s, and then rapidly decelerating, reaching zero velocity at 3.5 seconds. Yang et al. (2021) observed velocities ranging from 1.2 m/s to 2 m/s. Meanwhile, Zhang et al. (2021) conducted experiments using a small-scale flume model and combined it with three-dimensional discrete element method to interpret the experimental results, where the velocity of the debris flow ranged from 1.4 m/s to 3 m/s. Considering existing physical experiments and numerical simulations on small-scale flume models, it can be seen that the velocity of the debris flow in this study is similar to the relevant research results. When the debris flow passed the baffles near the source area at position P_1, the maximum speed reached 0.7 m/s, while the speed at position P_2 was 1.4 times that at P_1. From positions P_3 to P_5, the debris flow speed gradually increased to 1.5

times. The baffles at P_1 had the most significant impact on debris flow speed, reaching 61%, while the impacts at P_2 to P_5 were 50%, 31%, 17%, and 6%, respectively. This might be because, as the baffles were closer to the source area, the debris flow did not have enough time to accelerate. Therefore, the conclusion can be drawn: the closer the baffles are set to the source area, the greater the impact on the peak velocity of the debris flow. This is consistent with Lei et al. (2020), who installed baffles in the transit area to reduce the peak velocity of the debris flow.

Fig. 4(b) shows the change in kinetic energy of the debris flow when it passes through baffles at different positions. When the debris flow passed through the baffle, the kinetic energy exhibited four stages: slow increase, rapid increase, rapid decrease, and slow decrease until static accumulation. This aligns with the findings of Bi et al. (2018). Upon reaching the baffle, the debris flow experienced a peak in kinetic energy, irrespective of the baffle arrangement. Contact between the debris flow and the baffle resulted in a significant reduction in kinetic energy and duration of movement, indicating effective dissipation of the debris fragments' kinetic energy by the baffle. The kinetic energy of the debris flow was directly related to its destructive capacity, and different baffle positions led to varying losses in debris flow kinetic energy. When the baffle was positioned at P_1, where the debris flow had just started moving down the slope, its velocity and kinetic energy were relatively low. Hindered by the baffle after 0.5 seconds, the kinetic energy rapidly decreased, reaching zero at 1 second. The baffle at P_1 caused the shortest time for the debris flow's energy to drop to zero. The energy at P6 reached its maximum, being 4.5 times that of P_1. This indicates that the closer the baffle is to the ground, the greater the kinetic energy accumulated by the debris flow from top to bottom. The maximum kinetic energy followed the order: $P_6 > P_5 > P_4 > P_3 > P_2 > P_1$. The slope of the kinetic energy reduction curve varied, with P_1 having a slope of -0.87, and P_2 to P_6 having slopes of -1.11, -1.38, -1.8, -3.08, and -5.14, respectively. A larger maximum kinetic energy led to a faster reduction in kinetic energy after encountering the baffle. This is because baffle placement at a lower position is farther from the source area, resulting in a longer movement time and greater distance, leading to higher kinetic energy. Therefore, the baffle at P_6, positioned farther from the source area, allowed the debris flow to achieve higher speed, causing a rapid decrease in overall kinetic energy after

encountering the baffle. It can be observed that baffle placement closer to the source area resulted in a greater loss of kinetic energy for the debris flow, consistent with the results of Zhang et al. (2021). Baffles in the transit area contributed the most, while those in the deposition area were not fully utilized. Therefore, baffles constructed in the deposition area might not be the optimal arrangement.

3.1.2 Impact force on the first row of baffles

Fig. 5 shows the impact force on the first-row baffles with different baffle positions on debris flow. When baffles were set at position P_1, the debris flow exerted the maximum impact force on the first row of the baffle on the baffles. Specifically, the maximum impact force at P_1 was 1.33 times that at P_2, 1.81 times that at P_3, and 1.5 times that at P_4. This may be because, under the influence of gravity, the debris flow rushed out of the source area, positioning P_1 close to the source area. Most of the debris flow would impact the baffles, resulting in the maximum impact force on the baffles at P_1. When baffles were set at P_2 and P_3, some debris flow accumulated in the transit area, with the accumulation length at P_3 being greater than at P_2. After passing through the baffles, the debris flow decreased, leading to a smaller impact force on the baffles than at P_1. As for P_4, being set far from the source area, the debris flow had enough time to accelerate, resulting in a greater impact force on the baffles than at P_3.
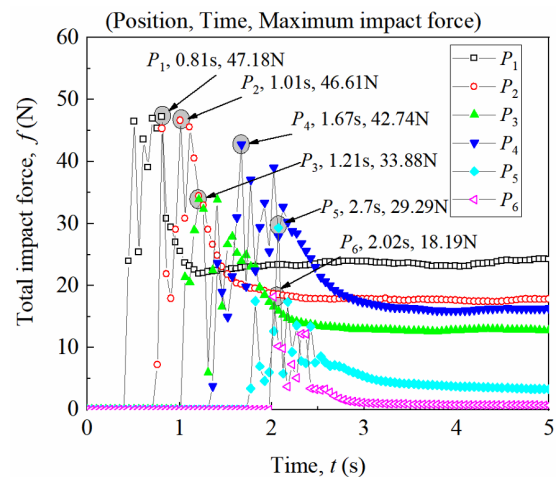

Fig. 5 The total impact force of the first row baffles with different baffle positions on debris flow.

In the transit area, the maximum impact force on the baffles set at P_2 was 1.87 times that on the baffles set in the deposition area at P_5 and 3.6 times that at P_6. With changes in the barrier placement, the impact

force on the first row of baffles initially decreased and then slightly increased, showing an overall decreasing trend. This is contrary to the situation observed by Zhang et al. (2020), where the first row of baffles in the de position area experienced higher impact forces (approximately 30% higher peak value compared to the first row of baffles in the transit area). It is important to note that in this study, 6 sets of baffles were selected at different positions. Overall, the impact force on the first row of baffles in the transit area was greater than that in the deposition area. Zhang et al. (2020) only considered two different positions for impact forces. When baffles are placed in the transit area, it is necessary to enhance the strength of the baffles, especially for those positioned near the source area, to prevent structural damage when debris flows through. Considering the analysis of baffles impact forces, the optimal placement positions may be P_3 and P_4 in the transit area and P_6 in the deposition area.

3.1.3 Debris flow accumulation form and mass

Fig. 6 shows the accumulation form and mass of debris flow before and behind the baffles Firstly, by comparing simulated results with and without baffles, it was observed that, in baffle-free particle simulation P_0, the debris flow exhibited a characteristic of concentrated distribution at the front end of the deposition area, forming a "ladle" shape. However, when baffles were placed in the transit area, their staggered arrangement significantly impeded the movement of the debris flow, thereby slowing down its velocity. Intercepted by the baffles, most of the debris flow accumulated behind the baffles, while a small portion of the debris flow moved downward along the transit area before the baffles. Upon reaching the deposition area, due to the lateral baffles' restriction, the debris flow immediately dissipated and spread forward, forming a fan-shaped deposition. Further observation of the deposition forms in Fig. 6(b, c, d, e, f) revealed that 80% of the debris flow accumulated in the transit area before the baffles, with only a small amount of debris flow distributed in the deposition area and the deposition is more dispersed. Additionally, the movement distance of the debris flow after passing through the baffles shortened as the baffles were placed closer to the bottom of the slope, with most of the debris flow concentrated at the front of the deposition area. Conversely, when baffles were placed near the source area, the movement distance of the debris flow after passing through the baffles became
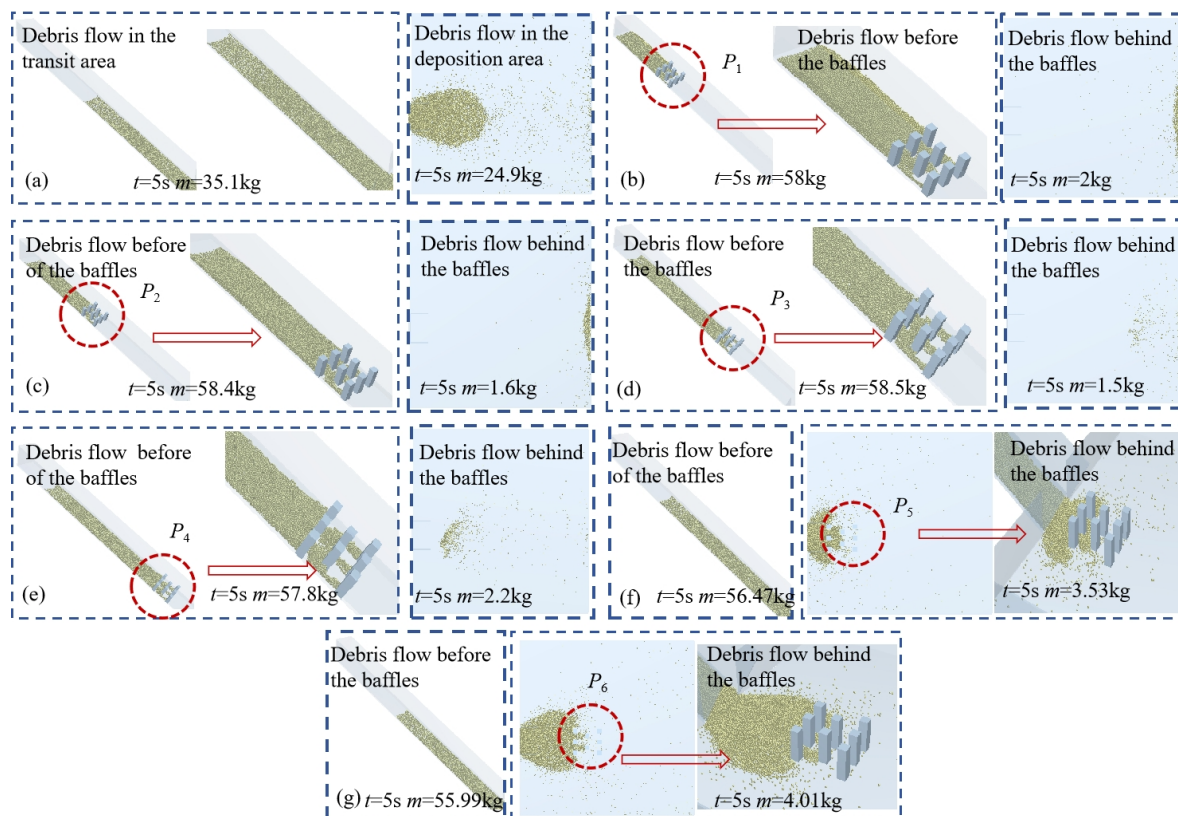

Fig. 6 Accumulation form and mass of debris flow before and behind the baffles: (a)P_0; (b) P_1; (c) P_2; (d) P_3; (e) P_4; (f) P_5; (g) P_6.

longer. It can be observed that the placement of baffles in the transit area and deposition area significantly altered the behavior of the debris flow.

Fig. 7 shows the mass of debris flow before and behind the baffles with different baffle positions. Fig. 7 illustrates the accumulation mass of the debris flows behind the baffles. Under the positions of P_1, P_2, P_3, P_4, P_5, and P_6, the mass of the debris flow behind the baffles was 2 kg, 1.6 kg, 1.5 kg, 2.2 kg, 3.53 kg, and 4.01 kg, respectively. This indicates that the interception effect of baffles placed in the transit area is superior to those placed in the deposition area. This is consistent with the research results of Zhang et al. (2021), which concluded that baffles set in the deposition area are more effective in blocking debris flows than those set in the transit area (approximately 10% larger debris flow deposition area). Considering the analysis of the accumulation mass and movement distance behind the baffles, the optimal placement positions are determined to be P_2, P_3 in the transit area, and P_5 in the deposition area.
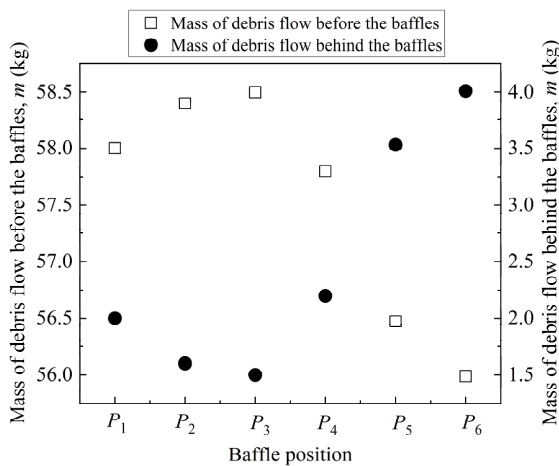

Fig. 7 Mass of debris flow before and behind the baffles with different baffle positions.

Considering the numerous positions for baffles in the transit area, a screening process was undertaken, resulting in the selection of two groups from the transit area and one group from the deposition area. Based on the consideration of debris flow accumulation before and behind the baffle, P_3, P_4, and P_5 were preliminarily chosen as the baffle deployment locations. Among these, P_4 was selected due to the substantial impact force on the first row of stakes for the baffle at P_2. The baffle at P_4 experienced lesser impact force, and the debris flow accumulation behind the baffle was also lower. Consequently, through comprehensive analysis, P_3, P_4, and P_5 were tentatively identified as the baffle positions.

## 3.2 Optimization of baffle parameters based on orthogonal experiments

3.2.1 Debris velocity and flow energy loss caused by baffles

Fig. 8(a) shows the velocity curve of debris flow in different cases. In the baffle-free particle simulation, it was observed by examining the time curves of *Control* 1, *Control* 2, and *Control* 3 that the velocity of the debris flow in the flow zone increased with the increase of the angle of the transit area. After reaching the peak velocity, the velocity decreased more rapidly with increasing angle. In Fig. 8(a), before the deceleration of the debris flow, the velocity-time curves of the debris flow in *Case* 1, *Case* 5, and *Case* 9 coincided, with a slope of 1.81; in *Case* 2, *Case* 6, and *Case* 7 the velocity-time curves coincided, with a slope of 2.69; in *Case* 3, *Case* 4 and *Case* 8, the velocity-time curves coincided, with a slope of 3.41. Additionally, the transit area angle for *Case* 1, *Case* 5, and *Case* 9 was 35°, for *Case* 2, *Case* 6, and *Case* 7 was 40°, and for *Case* 3, *Case* 4 and *Case* 8 was 45°. This indicates that the increase in the transit area angle, as observed in *Case* 1, *Case* 5, and *Case* 9 to *Case* 3, *Case* 4, and *Case* 8, possibly resulted from the greater gravitational potential energy due to the higher elevation of the source area from the ground, leading to higher velocities.

Fig. 8(b) shows the kinetic energy curve of debris flow in different cases. In the baffle-free particle simulation, it was observed that the kinetic energy of the debris flow in the flow channel increased as the angle of the transit area increased, based on the kinetic energy curves of *Control* 1, *Control* 2, and *Control* 3. The impact of different arrangements of baffles on the kinetic energy of the debris flow and the variation in debris flow velocity was consistent. For instance, in *Case* 8, the debris flow reached its maximum kinetic energy of 173 J at 1.25 seconds, whereas in *Case* 1, the maximum kinetic energy was 39J. This could be attributed to the fact that in *Case* 8, the baffles were positioned far from the source area, and the inclination angle of the transit area in the transit area was large. Conversely, in *Case* 5 and *Case* 9, the transit area angle of the transit area was smaller, resulting in the debris flow acquiring less kinetic energy.

3.2.2 Impact force on the first row baffles

Fig. 9 shows the total impact force of the first-row
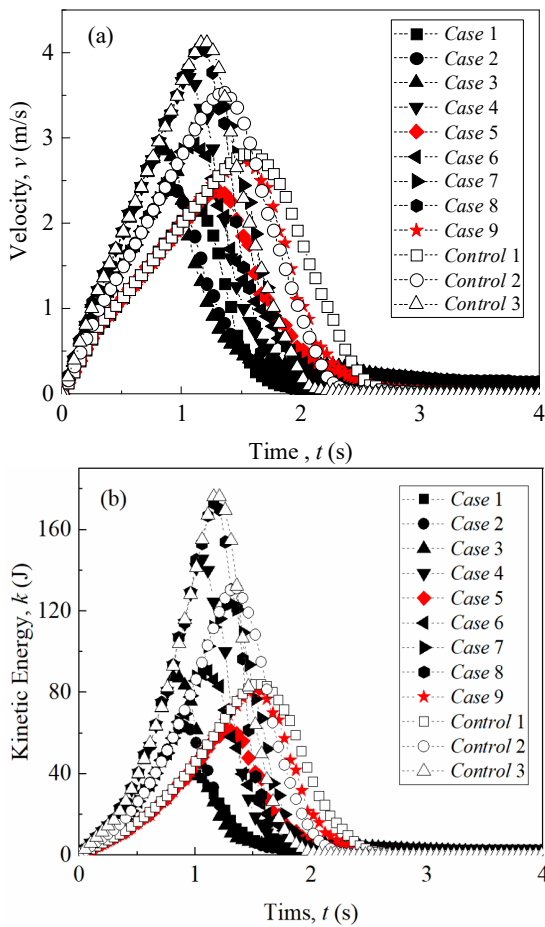
Fig. 8 (a) Velocity and (b) kinetic energy of debris flow in different cases.
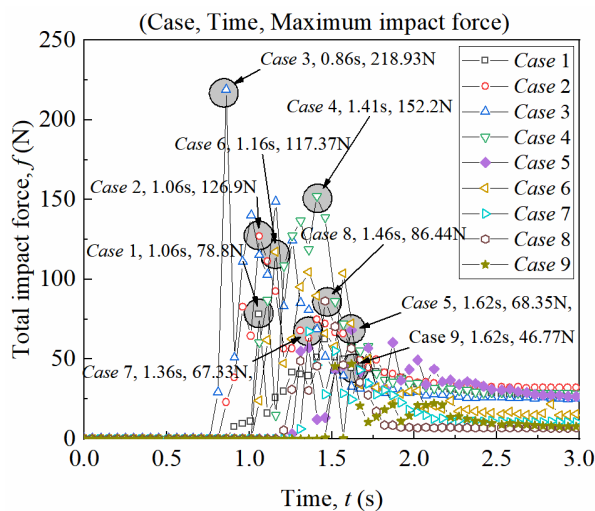
Fig. 9 The total impact force of the first row baffles in different cases.

baffles in different case. Based on the data from Fig. 9, when baffles were arranged in the transit area, the maximum impact force on the first row of baffles in

Case 3 was approximately 218.72N. In contrast, in *Case* 5, the minimum impact force on the first row of baffles was 68.35N. Additionally, it is noteworthy that the impact force on the first row of baffles in *Case* 3 was 3.2 times that in *Case* 5. Further observations from experiments in *Case* 1, *Case* 2, *Case* 4, and *Case* 6 indicated impact forces on the first row of baffles as 78.8N, 126.7N, 152.2N, and 117.37N, respectively. Overall, when baffles were arranged in the transit area, *Case* 5 had the smallest impact force on the first row of baffles. When baffles were located in the deposition area, the arrangement of baffles in *Case* 9 resulted in the smallest impact force on the first row of baffles. In this case, the impact forces on the first row of baffles in *Cases* 7 and *Cases* 8 were 1.43 times and 1.8 times that of *Case* 9, respectively. This may be attributed to the increase in the angle of the transit area, leading to higher elevation at the source and an increase in debris flow velocity.
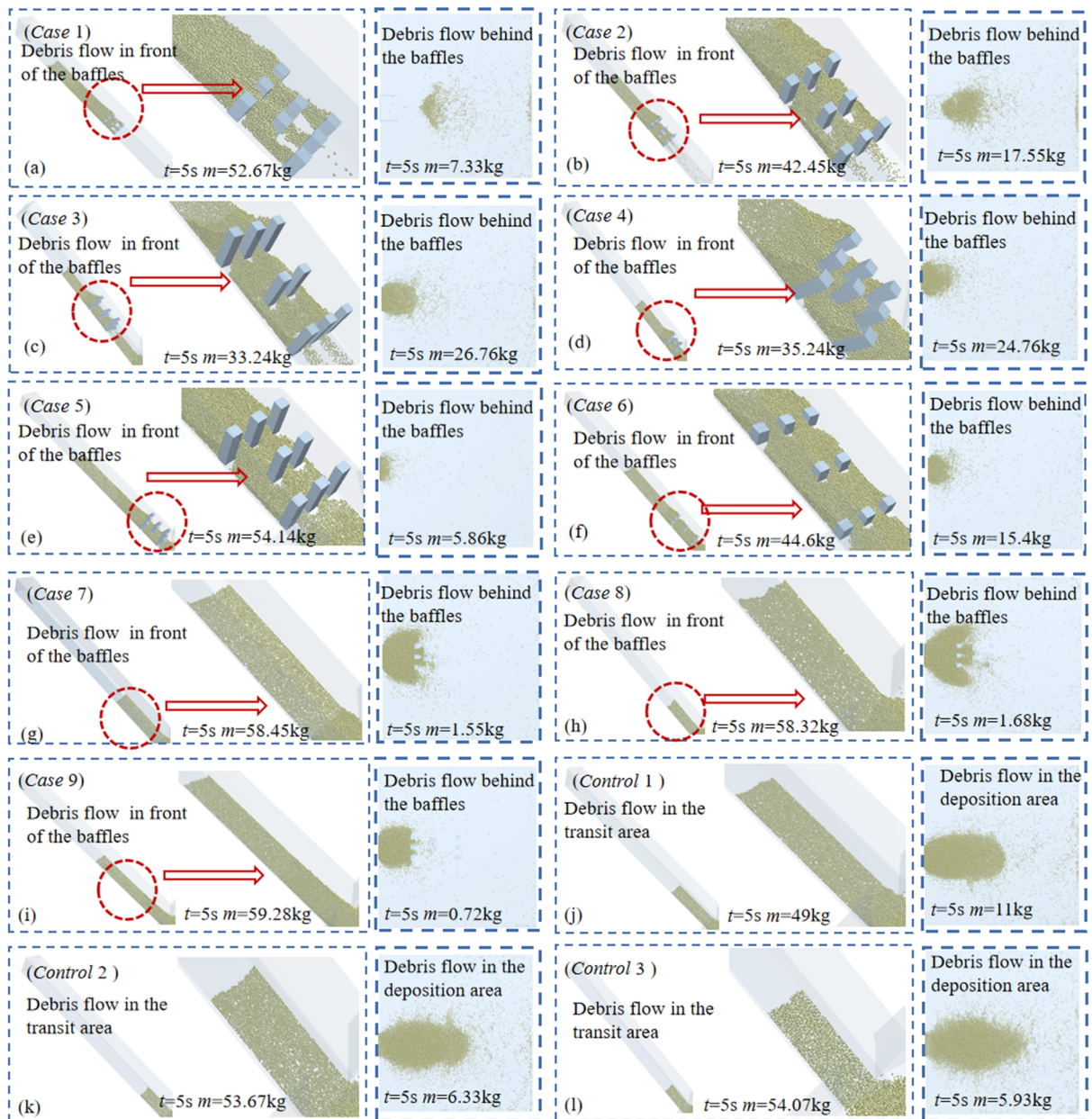
3.2.3 Debris flow accumulation form and mass

Fig. 10 shows the accumulation form and mass of debris flow before and behind the baffles. In the baffle-free particle simulation, by observing *Control* 1, *Control* 2, and *Control* 3, we found that as the angle of the transit area increased, the accumulation length of the debris flow in the flow passage gradually decreased, while the distribution area in the deposition area gradually expanded. From Fig. 10, it can be observed that, under different configurations of baffle arrangements, there were noticeable changes in the deposition patterns and distances of debris flows in the deposition area after passing through the baffles. Specifically, in *Case* 1 and *Case* 3, where baffles were placed in the transit area, the debris flow was distributed in the middle and front of the deposition area, appearing dispersed. In *Case* 4, *Case* 5, and *Case* 6, the arrangement of baffles caused the debris flow to concentrate more at the front of the deposition area. Meanwhile, in *Case* 7, *Case* 8, and *Case* 9, the baffles exhibited a fan-shaped distribution.

Fig. 11 shows the mass of debris flow before and behind the baffles in different cases. The experimental results from Fig. 11 indicate that the baffles were effective in blocking debris flows. In all experiments, the mass of debris flows behind the baffles in *Case* 3 was the highest, reaching up to 26.76 kg. *Case* 7 and *Case* 9 experiments achieved the best blocking effects, with masses of 1.54 kg and 0.71 kg, respectively. Therefore, it can be concluded that the configuration of

Fig. 10 Accumulation form and mass of debris flow before and behind the baffles: (a) *Case* 1; (b) *Case* 2; (c) *Case* 3; (d) *Case* 4; (e) *Case* 5; (f) *Case* 6; (g) *Case* 7; (h) *Case* 8; (i) *Case* 9; (j) *Control* 1; (k) *Control* 2; (l) *Control* 3.

the baffles significantly influences the deposition patterns, distances, and blocking effects of debris flows.

3.2.4 Orthogonal experimental mean and range value

Table 4 shows the mean and range of parameters of the orthogonal experiment. K_i in the table represents the average of each index data of repeated experiments at each level. By comparing the values of K_i, the optimal level of each factor can be determined. In addition, the range R is the difference between the maximum value and the minimum value of the mean, which is used to

indicate the degree of influence of factors. When the range is larger, it means that the influence of this factor is also greater. According to the range (R) values in Table 4, the following conclusions can be drawn: For the impact force of debris flow on the first-row baffle, the influence of the four factors, in decreasing order, is as follows: $\alpha > P > S_r > h$. For the mass of debris flows behind the baffle, the influence of the four factors, in decreasing order, is as follows: $P > \alpha > S_r > h$. Fig. 12 shows the degree of influence of each factor on the experimental results under the 4-factor 3-level orthogonal experiment. Observing Fig. 12, we can see
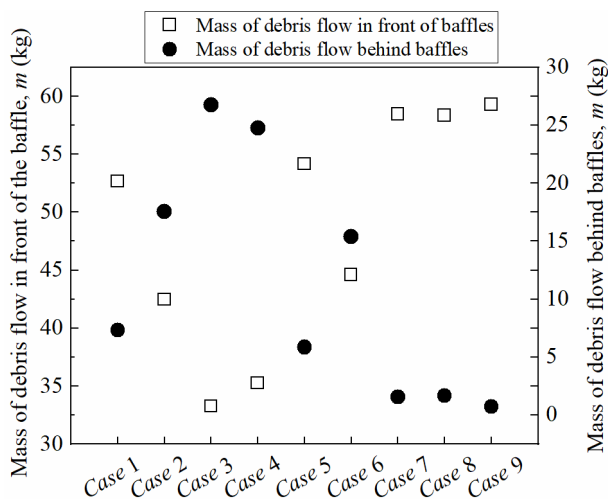
Fig. 11 Mass of debris flow before and behind the baffles in different cases.

Table 4 Analyze the mean and range of parameters

Analytical parameters	K_i and R	Baffle			Angle of transit area
		Position	Row spacing	Height	
f (N)	K_1	141.499	99.443	94.203	64.640
	K_2	112.640	93.922	108.649	103.892
	K_3	66.847	127.620	118.133	152.453
	R	74.652	33.698	23.930	87.813
m (kg)	K_1	17.210	11.209	8.133	4.630
	K_2	15.340	8.361	14.341	11.498
	K_3	1.311	14.291	11.387	17.733
	R	15.899	5.930	6.208	13.103

Note: f, the maximum impact force of the first baffle; m, debris flow mass behind the baffle; K_i, mean value; R, range value.

that, in terms of evaluating the impact force on the first-row baffle and the accumulated mass of debris flow behind the baffle, the optimal combinations obtained from the orthogonal experiment simulation were P_5, S_r=16, α=35°, h=9.

4 Discussion

The arrangement of baffles influenced the velocity and kinetic energy of debris flow (Teufelsbauer et al. 2011; Luo and Senetakis 2022; Bi et al. 2022). Debris flow velocity showed multi-stage changes under the influence of baffles at different locations (Wang et al. 2021; Liu et al. 2019). The closer the baffles were set to the source area, the greater the influence on the peak velocity of the debris flow. This is consistent with Lei et al. (2020), who arranged baffles in the flow zone to reduce the peak velocity of debris flow. As the debris

flow passed through the baffles, the kinetic energy exhibited four stages of slow increase, rapid increase, rapid decrease, and slow decrease until static accumulation. This is consistent with the conclusion of Bi et al. (2018). The closer the baffles were set to the source area, the greater the degree of energy dissipation of the debris flow, consistent with the results of Zhang et al. (2021).

The arrangement of baffles affected the impact force of debris flow on the baffles (Zhang et al. 2021; Huang et al. 2021; Zhang and Huang 2022; Chen et al. 2022). This study found that as the position of the baffle arrangement changed, the impact force on the first row of baffles decreased slightly and then slightly increased, showing an overall decreasing trend (He et al. 2016). This is contrary to the observation by Zhang et al. (2020) of larger impact forces on the first row of baffles in the accumulation zone (peaking at about 30% of the first row of baffles in the flow zone). This may be because this study selected six groups of baffles at different positions, overall the total impact force on the first row of baffles in the transit area was greater than that in the deposition area, whereas Zhang et al. (2020) only considered impact forces at two different positions.

The arrangement of baffles affected the accumulation form and mass of debris flow (Bi et al. 2021; Luo et al. 2023; Wang et al. 2020a). Goodwin et al. (2020) found through discrete element method studies that for a given Froude number, particle size, and baffle spacing, baffles in the flow zone were less efficient in intercepting debris flow compared to those in the deposition area, consistent with the results of this study. When baffles were set in the flow zone, 80% of the debris flow accumulated before the baffles, with only a small amount of debris flow distributed in the accumulation zone and the accumulation being more dispersed. Setting baffles in the flow zone significantly changed the deposition morphology and quality of debris flow compared to setting them in the deposition area (Gan et al. 2018). This is consistent with the results of Z hang et al. (2020), who set up baffles on slopes and platforms and found that baffle placement significantly affected the sedimentation characteristics of granular flow. The distance traveled by debris flow after passing through the baffles shortened as the baffles were placed closer to the bottom of the slope, with most of the debris flow concentrated in the front of the deposition area. Conversely, when the baffles were located near the source area, the distance traveled
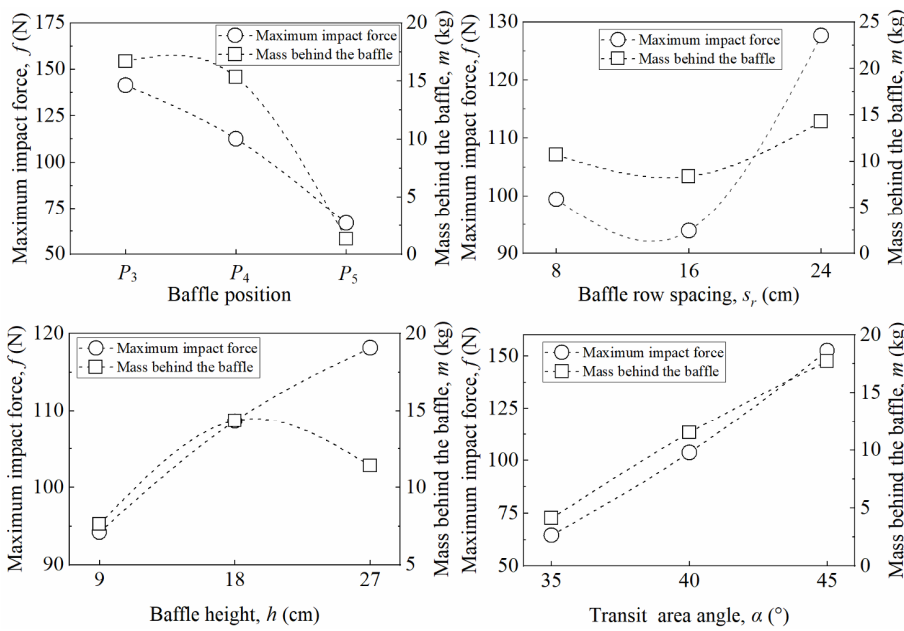
Fig. 12 Influence of different baffle positions, baffle row spacing, baffle height and transit area angle on the maximum impact force of the baffles and the mass of debris flow behind the baffle.

by the debris flow after passing through the baffles became longer. This is contrary to the results of Zhang et al. (2020), who set up piles on platforms, where the axial jumping distance and lateral extension of the debris flow significantly decreased after passing through the baffle structure, possibly due to differences in factors such as the angle setting and parameters of the flow zone.

The present study conducted numerical simulations based on a small-scale flume model but did not compare with flume model experiments. Due to the scale effect of flume models, their applicability to engineering practice may be limited. Future work will utilize the experimental results of this study for verification through flume model experiments and conduct simulations at real scales to improve the accuracy of the simulation results.

5 Conclusions

This study employed the DEM to thoroughly investigate the effects of baffle position, baffle row spacing, baffle height, and transit area angle on the interaction between debris flow and baffles. Firstly, through single-factor experiments, the impact of baffles at different positions on debris flow velocity and kinetic energy was explored. The selected baffle

deployment positions were preliminarily selected, taking into account both the impact force of debris flow on the first-row baffle and the mass and form of debris flow accumulation. Subsequently, based on multi-factor experiments, the combined effects of baffle position, height, row spacing, and transit area angle on the protective effect of baffles against debris flow were investigated. The optimal baffle deployment configurations were determined through mean and range analyses. Based on the results, the following conclusions could be drawn:

(1) Different positions of the baffles exhibited distinct kinetic energy evolution patterns during various stages of debris flow deceleration. The baffles in the transit area region began reducing the velocity of debris flow before reaching its peak, whereas the baffles in the deposition area only started reducing the velocity of debris flow when it approached the velocity peak. Additionally, the maximum energy dissipation produced by the baffle structure at position P_1 in the transit area region accounted for 81.25% of the free-flow energy, while the minimum energy dissipation at position P_4 was 29.17% of the free-flow energy. This indicates that the baffles in the transit area region effectively reduced debris flow velocity and dissipated its kinetic energy.

(2) In the single-factor experiment, the impact forces experienced by the baffles at different positions varied when intercepting the debris flow. Generally speaking, the impact forces on the baffles placed within the flow area were greater than those on the first row of baffles placed in the deposition area. The best debris flow mass interception effect was observed when the baffles were set at P_3, whereas the poorest effect was observed when set at P_6. Baffles positioned in the flow area exhibited a better mass interception effect on the debris flow compared to those positioned in the deposition area, but they had to endure greater impact forces.

(3) Under the combined influence of baffle

position, baffle row spacing, baffle height, and transit area angle, the interception effectiveness of the baffles on debris flows could be significantly altered. Through variance analysis based on orthogonal design experiments, it was found that the arrangement of baffles had a substantial impact on both the accumulation mass and form of debris flows. When evaluating the first-row baffle pressure, the factors, in descending order of influence, were transit area angle (α) > baffle position (P) > baffle row spacing (S_r) > baffle height (h). Evaluating the mass of debris flows behind the baffles, the factors, from most to least influential, were $P > \alpha > S_r > h$. The optimal combinations identified in this orthogonal experiment simulation were consistently P_5, h=9, S_r=16, and α=35°.

Acknowledgments

Author Contribution

SUN XinPo: Conceptualization, Writing - Original Draft, Funding acquisition; CHEN Min: Writing - Original Draft, Writing - Review & Editing; BI Yuzhang: Methodology, Software, Writing - Review & Editing; ZHENG Lu: Formal analysis, Funding acquisition; CHE Chi: Visualization; XU Ao: Formal analysis; Tian Zi-Jian: Writing - Review & Editing; JIANG Zheyuan: Writing - Review & Editing, Supervision, Project administration.

Ethics Declarations

Availability of Data/Materials: The datasets obtained during the experimental investigation are available upon reasonable request from the relevant author.

Conflicts of Interest: The authors declare no conflicts of interest.

References

Bi YZ, He SM, Li XP, et al. (2016) Geo-engineered buffer capacity of two-layered absorbing system under the impact of rock avalanches based on Discrete Element Method. J Mt Sci 13(5): 917-929. https://doi.org/10.1007/s11629-014-3354-0

Bi YZ, Sun XP, Zhao H, et al. (2021) Comparison regarding the effects of different baffle systems as impacted by rock avalanches. Int J Civ Eng 19:127-144. https://doi.org/10.1007/s40999-020-00557-w

Bi YZ, Wang DP, Yan SX, et al. (2023) Research on the blocking effect of baffle-net structure on rock avalanches: consider the influence of particle splashing. Bull Eng Geol Environ 82, 277. https://doi.org/10.1007/s10064-023-03289-y

Bi YZ, Wang DP, Fu Xl, et al. (2022) Optimal array layout of cylindrical baffles to reduce energy of rock avalanche. J Mt Sci 19(2): 493-512. https://doi.org/10.1007/s11629-021-6916-y

Bi YZ, Du YJ, He SM, et al. (2018) Numerical analysis of effect of baffle configuration on impact force exerted from rock avalanches. Landslides 15: 1029-1043. https://doi.org/10.1007/s10346-018-0979-z

Cheng H, Zhang B, Huang Y (2022) SPH-based numerical study on the influence of baffle height and inclination on the interaction between granular flows and baffles. Water 14(19):3063. https://doi.org/10.3390/w14193063

Cheng H, Han PF, Su YW (2020) Sliding and accumulation characteristics of loose materials and its influencing factors based on discrete element method. Acta Phys Sin 69(16): 164501. https://doi.org/10.7498/aps.69.20200223

Choi CE, Ng CWW, Song D, et al. (2014) Flume investigation of landslide debris-resisting baffles. Can Geotech J 51(5): 540-553. https://doi.org/10.1139/cgj-2013-0115

Cuomo S, Cascini L, Pastor M, et al. (2017) Modelling the propagation of debris avalanches in presence of obstacles. In: Mikoš M, Arbanas Ž, Yin Y, Sassa K (eds) Advancing Culture of Living with Landslides. WLF 2017. Springer, Cham. https://doi.org/10.1007/978-3-319-53487-9_55

Cuomo S, Petrosino S (2020) Two control works to counteract the inception of debris avalanches. In: Calvetti, F., Cotecchia F, Galli A, Jommi C (eds) Geotechnical Research for Land Protection and Development. CNRIG 2019. Lecture Notes in Civil Engineering, vol 40. Springer, Cham. https://doi.org/10.1007/978-3-030-21359-6_8

Cuomo S, Moretti S, Frigo L, et al. (2021) Performances of geosynthetics-reinforced barriers for protection against debris avalanches. In: Vilímek V, Wang F, Strom A, et al. (eds) Understanding and Reducing Landslide Disaster Risk. WLF 2020. ICL Contribution to Landslide Disaster Risk Reduction. Springer, Cham. https://doi.org/10.1007/978-3-030-60319-9_38

Gan BR, Yang XG, Chen ML, et al. (2018) Effects of fine particle content and sample scale on the failure properties of loose landslide deposits. Arab J Geosci 11(7): 152. https://doi.org/10.1007/s12517-018-3481-y

Goodwin GR, Choi CE, Yune CY (2021) Towards rational use of baffle arrays on sloped and horizontal terrain for filtering boulders. Can Geotech J 58(10): 1571-1589. https://doi.org/10.1139/cgj-2020-0363

He S, Liu W, Li X (2016) Prediction of impact force of debris flows based on distribution and size of particles. Environ Earth Sci 75(4):298. https://doi.org/10.1007/s12665-015-5180-2

Huang Y, Zhang B, Zhu C (2021) Computational assessment of baffle performance against rapid granular flows. Landslides 18:

485-501.
https://doi.org/10.1007/s10346-020-01511-6

Huang Y, Shi H, Zhang B. (2023) Crown-like baffle system against rock avalanches: energy dissipation mechanism and numerical verification. J Earth Sci 34: 304-315.
https://doi.org/10.1007/s12583-021-1571-3

Kim BJ, Yune CY (2020) Flume investigation of cylindrical baffles on landslide debris energy dissipation. Landslides 19: 3043-3060.
https://doi.org/10.1007/s10346-022-01945-0

Kim BJ, Kim HS, Choi CE, et al. (2019) An experimental study on cylindrical countermeasures for dissipation of debris flow energy. J Korean Geosynth So 20(1): 57-65.
https://doi.org/10.14481/jkges.2019.20.1.57

Kim BJ, Kim D, Yune CY (2022) Experimental study on the impact dynamics of cylindrical baffles with a rigid barrier against debris flows. Appl Sci 12(17):8632.
https://doi.org/10.3390/app12178632

Luo G, Chen W, Shen W, et al. (2023) Influence of submerged sill on the deposition and energy dissipation of granular flow. Bull Eng Geol Environ 82(7): 1-15.
https://doi.org/10.1007/s10064-023-03269-2

Lei M, Yang P, Wang Yk, et al. (2020) Numerical analyses of the influence of baffles on the dynamics of debris flow in a gully. Arab J Geosci 13, 1052.
https://doi.org/10.1007/s12517-020-06016-z

Lei M, Xu ZX, Wang YK, et al. (2020) Dynamic mechanism of three-dimensional mixed-size grain/bed collision on non-flat bed using discrete element method. Arab J Geosci 13(2): 71.
https://doi.org/10.1007/s12517-019-5003-y

Liu W, Wang DP, Zhou JW, et al. (2019) Simulating the Xinmo landslide runout considering entrainment effect. Environ Earth Sci 78: 585.
https://doi.org/10.1007/s12665-019-8596-2

Liu HD, Li DD, Wang ZF (2018) Dynamic process of the Wenjiagou rock landslide in Sichuan Province, China. Arab J Geosci 11(10): 233.
https://doi.org/10.1007/s12517-018-3564-9

Luo L, Senetakis K (2022) Influence of analog barrier type and impact velocity on the energy dissipation of simulant saprolitic rock particles colliding rigid and deformable barrier systems. Transp Geotech 35, 100784.
https://doi.org/10.1016/j.trgeo.2022.100784

Moretti S, Cuomo S, Aversa S (2020) Feasibility of foothill barriers to reduce the propagation of debris flows. In: Calvetti F, Cotecchia F, Galli A, Jommi C (eds) Geotechnical Research for Land Protection and Development. CNRIG 2019. Lecture Notes in Civil Engineering, vol 40. Springer, Cham.
https://doi.org/10.1007/978-3-030-21359-6_33

Pu J, Huang Y, Guo Z, et al. (2024) Physical vulnerability of reinforced concrete buildings under debris avalanche impact based on GF-discrepancy and DEM-FEM. Nat Hazards 120: 2571-2597.
https://doi.org/10.1007/s11069-023-06294-2

Scheidl C, Friedl C, Reider L, et al. (2023) Impact dynamics of granular debris flows based on a small-scale physical model. Acta Geotech 1-19.
https://doi.org/10.1007/s11440-023-02116-8

Song D, Choi CE, Ng CWW, et al. (2018) Geophysical flows impacting a flexible barrier: effects of solid-fluid interaction. Landslides 15: 99-110.
https://doi.org/10.1007/s10346-017-0856-1

Teufelsbauer H, Wang Y, Pudasaini SP, et al. (2011) DEM simulation of impact force exerted by granular flow on rigid structures. Acta Geotech 6: 119-133.
https://doi.org/10.1007/s11440-011-0140-9

Wang DP, Li Q, Bi YZ, et al. (2020a) Effects of new baffles system under the impact of rock avalanches. Eng Geol 264:255-261.
https://doi.org/10.1016/j.enggeo.2019.105261

Wang DP, Li QZ, Bi YZ, et al. (2020b) Optimal layout of a new type of baffle based on high-risk areas of rock avalanches. Rock Soil Mech 41(4): 1323-1332.
https://doi.org/10.16285/j.rsm.2019.0721 (in Chinese)

Wang F, Chen X, Chen J, et al. (2017) Experimental study on a debris-flow drainage channel with different types of energy dissipation baffles. Eng Geol 220: 43-51.
https://doi.org/10.1016/j.enggeo.2017.01.014

Wang F, Wang J, Chen X, et al. (2021) Experimental study on debris-flow velocity control mechanism with baffles in a drainage channel. Bull Eng Geol Environ 80, 5203-5217.
https://doi.org/10.1007/s10064-020-02086-1

Yang H, Wei F, Hu K (2014) Mean velocity estimation of viscous debris flows. J Earth Sci 25: 771-778.
https://doi.org/10.1007/s12583-014-0465-z

Yang HQ, Emdadul MD, Song KL (2021) Experimental study on the effects of physical conditions on the interaction between debris flow and baffles. Phys Fluids 33 (5): 056601.
https://doi.org/10.1063/5.0046670

Zhang B, Huang Y, Liu J (2021) Micro-mechanism and efficiency of baffle structure in deceleration of granular flows. Acta Geotech 16: 3667-3688.
https://doi.org/10.1007/s11440-021-01290-x

Zhang B, Huang Y (2022) Impact behavior of super speed granular flow: Insights from centrifuge modeling and DEM simulation. Eng Geol 299, 106569.
https://doi.org/10.1016/j.enggeo.2022.106569

Zhang ZY, Jin XG, Bi J (2019) Development of an SPH-based method to simulate the progressive failure of cohesive soil slope. Environ Earth Sci 78: 537.
https://doi.org/10.1007/s12665-019-8507-6

Zhao C, Fu CH (2017) Numerical simulation of movement characteristics of debris flow based on DEM. Adv Sci Technol Water Res 37(2): 43-47.
https://doi.org/10.3880/j.jssn.1006-7647 (In Chinese)

Zhao T, Utili S, Crosta GB (2015) Rockslide and impulse wave modelling in the Vajont reservoir by DEM-CFD analyses. Rock Mech Rock Eng 49(6): 2437-2456.
https://doi.org/10.1007/s00603-015-0731-0

Zhou C, Hu HS, Song D, et al. (2019) Experimental study on the regulation function of slit dam against debris flows. Landslides 16: 75-90.
https://doi.org/10.1007/s10346-018-1065-2

Zhou GD, Du J, Song D. et al. (2020) Numerical study of granular debris flow run-up against slit dams by discrete element method. Landslides 17, 585-595.
https://doi.org/10.1007/s10346-019-01287-4

Zhu CQ, Huang Y, Zhan LT (2018) SPH-based simulation of flow process of a landslide at Hongao landfill in China. Nat Hazards. 93(3): 1113-1126.
https://doi.org/10.1007/s11069-018-3342-8

Zhu CQ, Huang Y, Sun J (2020) Solid-like and liquid-like granular flows on inclined surfaces under vibration-Implications for earthquake-induced landslides. Comput Geotech 123: 103598.
https://doi.org/10.1016/j.compgeo.2020.103598